Journal of Micromechanics and Microengineering

PAPER

Propulsion reversal in oscillating-bubble powered micro swimmer

IOP Publishing
Journal of Micromechanics and Microengineering
J. Micromech. Microeng. **31** (2021) 084001 (9pp)
https://doi.org/10.1088/1361-6439/ac0e7f

Propulsion reversal in oscillating-bubble powered micro swimmer

Fang-Wei Liu[1], Ye Zhan[1,2] and Sung Kwon Cho[1,*]

[1] Department of Mechanical Engineering and Materials Science, University of Pittsburgh, Pittsburgh, PA, United States of America
[2] Currently with Qualcomm Technologies, Inc., Buffalo, NY, United States of America

E-mail: skcho@pitt.edu

Received 4 April 2021, revised 9 June 2021
Accepted for publication 24 June 2021
Published 7 July 2021

Abstract

A gaseous bubble trapped in a one-end-open tube generates a microstreaming flow when oscillated by externally excited acoustic waves, which has been proven as an effective propulsion force for underwater micro robots. The propulsion force is known to be a pushing force on the tube since the microstreaming flow is outgoing from the tube exit. This article reports that this microstreaming flow and thus propulsion direction can be reversed when the gas–liquid interface of the bubble is exposed outside of the tube, which is confirmed using two types of tubes: commercially available capillary tubes and microfabricated parylene tubes. This result implies that control of the interface position in the tube relative to the exit is critically important. As such, two methods are incorporated to control the position of the interface and thus the length of trapped bubble: neck structure at the tube exit and plasma treatment of the tube. The neck structures enable the three-phase contact line to pin at the neck, thus providing uniform bubble lengths and warranting consistent oscillation spectra and propulsion behaviors. However, the reversal in microstreaming flow and propulsion does not occur since the bubble interface with the neck structure still stays inside the tube. The plasma treatment makes the three-phase contact line pinned right at the tube exit such that the entire interface is exposed to the outside of the tube. In this case, the reversal in microstreaming and propulsion consistently occurs, which provides an additional option to control the propulsion and steering of micro swimmers powered by acoustically oscillating bubbles.

Supplementary material for this article is available online

Keywords: microstreaming, acoustofluidics, micro robot

(Some figures may appear in colour only in the online journal)

1. Introduction

A gaseous bubble in a liquid environment oscillates when it is exposed to pressure waves. The oscillating interface of the bubble produces a local flow field around the bubble surface, known as microstreaming. The study of fluid dynamics in response to the collapse of a spherical bubble was pioneered in the early 19th century by Rayleigh, who derived the equation of the interface dynamics [1]. Rayleigh's work has been continuously improved and modified, finally culminating in the Rayleigh-Plesset-Noltingk-Neppiras-Poritsky (RPNNP) equation describing the interface motion with an oscillating spherical bubble [2]. Nyborg and Lighthill studied acoustically induced flows in liquid [3], in the vicinity of an solid–fluid interface [4] and around a resonant gas bubble [5]. Later, the resonance frequency of an oscillating bubble, where the oscillation amplitude reaches maximum, was determined by the conformation and the size of the bubble [6, 7]. However, for a while since the RPNNP equation and the above Nyborg and Lighthill's works were reported, the application of such oscillating micro bubbles has not been explored extensively

[*] Author to whom any correspondence should be addressed.

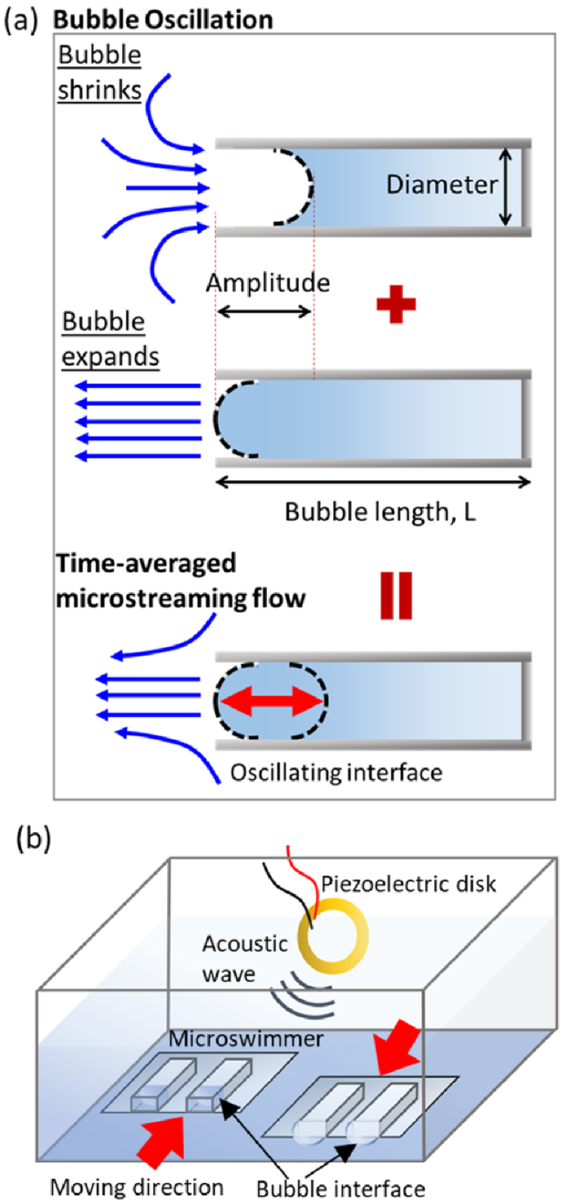

Figure 1. (a) The working principle of micro swimmer by microstreaming. The micro swimmer is propelled by the gaseous bubbles trapped in the micro tubes which are excited by the acoustic wave generated from the piezoelectric disk. (b) The oscillation of bubbles produce a significant propulsive force whose direction is determined by the position of the bubble interface. The arrows indicate the propulsion directions.

due to the limited access to small scale. Past decades since microelectromechanical systems and microfluidics technologies emerged and offered a direct access to and precise control in micro scale, oscillating micro bubbles have been widely utilized to actuate and control local fluid motions in micro scale. For example, the microstreaming induced by oscillating bubbles has been used to pump [8–10] and mix [11–16] micro fluids. The drag forces induced by microstreaming, sometimes combined with the acoustic radiation forces emitted by oscillating bubbles, have been used to handle, transport, and filter micro objects such as micro particles, cells and micro-organisms [17–23].

In addition to the manipulations of local flow field as well as small objects, microstreaming can create strong forces to propel solid objects at micro scale. In micro scale or in the low Reynolds number flow regime, the conventional propulsion principles efficient at macro scale would not be always effective due to the dominant viscous effects [24]. For example, when a gaseous bubble trapped in a one-end-open micro tube is oscillated by an external acoustic wave, the oscillating bubble generates cyclic flows of intake and exhaust near the tube exit at the frequency of the acoustic wave. In case that the oscillating frequency ω is low, that is, the Reynolds number (more exactly, oscillating Reynolds number, $\mathrm{Re}_{\mathrm{osc}} = \frac{\rho\omega a D}{\mu}$, where a is the oscillation amplitude, and ρ and μ the density and viscosity of the liquid) is low, the flow becomes reversible: the streamlines of the intake and exhaust flows would be almost identical except their directions are opposite to each other. As a result, the intake and exhaust flows are cancelled out, and neither the time-averaged net flow nor propulsion is generated [25]. However, when the oscillating frequency is high enough, patterns of the intake and exhaust flows become asymmetric since the inertia effects come into play (figure 1(a)). In this situation, a non-zero time-averaged net flow is generated mainly in the axial direction from the tube opening (generally in the outgoing direction), thus exerting a reactionary propulsion force on the tube, opposite to the flow direction. Such propulsion force can be employed to propel mobile miniature devices, like micro swimmers, in order to possibly navigate inside human body. Micro swimmers show a great potential in biomedical applications including target drug delivery, minimal invasive micro surgery, biosensing, etc [26].

This propulsion method provides the unique advantages of untethered, remote, wireless excitation with no or minimal harm to human body. The first attempt to adopt the propulsion principle for mobile devices was made by Dijkink *et al* [27] using a one-end-open capillary tube, coined 'acoustic scallop'. Then, Feng *et al* developed this principle in micro scale and fabricated micro swimmers utilizing the microfabrication technology [25, 28]. In addition, they numerically and experimentally analyzed microstreaming propulsion with the microfabricated swimmers. The propulsion force is proportional to the oscillation amplitude and frequency of the bubble interface near the tube opening. Later, this principle was further applied to propel and steer micro swimmers in 2D [29, 30] and even 3D space [31, 32]. To steer the micro swimmers, multiple bubbles embedded in the micro swimmer body with different alignments were resonated at different frequencies. By matching the excitation frequencies with the resonance frequencies of the selected bubbles [25, 28–33], the micro swimmer can change the swimming direction and thus steer along the programmed path in a 2D as well as 3D space. Furthermore, this directional microstreaming flow combined with acoustic radiation forces from oscillating bubbles has been employed to propel micro carriers [34, 35].

In all the above studies, the directions of axial microstreaming flows were always outgoing from the tube opening, and thus the generated propulsion forces were in the direction from the tube opening end towards the tube closing end. That is, the microstreaming flow pushed the micro tubes. In this paper, however, we report that the direction of microstreaming flow and thus the propelling force can be reversed (i.e. generates a pulling force) depending on the bubble interface location with respect to the tube exit. As illustrated in figure 1(b), when the bubble interface is located deep inside the tube, the swimmer likely propels opposite to the tube opening; while the propulsion direction can be reversed when the interface of the bubble is exposed to the outside of the tube opening.

This finding implies that controlling the location of bubble interface is critically important. This importance is even more emphasized, considering that the bubble length critically affects the resonance frequency of the trapped bubble. In the previous studies, a dried micro tube was simply submerged in water to trap and keep a gaseous bubble in the micro tube utilizing the hydrophobicity of the tube inner surface.

However, this trapping method showed a significant variation in the length of trapped bubbles. As a result, the bubbles trapped in the tubes (although the tube lengths are kept the same) showed inconsistent resonance behaviors. So far, fine control methods have not or rarely been implemented to make the bubble length uniform. Hence, the major focus of this paper is two-fold: (a) studying the effect of the interface location on propulsion reversal; (b) developing methods to fix the bubble interface at a desired location in the tube and to make the bubble length more consistent and uniform. For the first part, two types of tubes, capillary tubes and microfabricated tubes, are examined to study the reveral of flow and propulsion. In the second part, two methods are implemented to anchor the the three-phase contact line of the bubble interface: introducing a neck structure and treating the surface with plasma at the tube exit area. Detailed designs and experimental results are presented in the next sections.

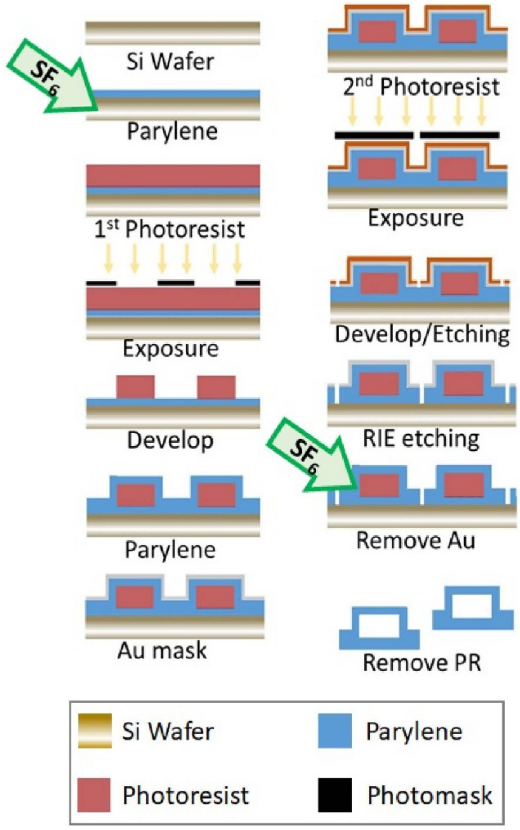

Figure 2. The fabrication process flow of microfabricated micro swimmer. The green arrows indicate SF6 plasma treatments to enhance hydrophobicity, resulting in pinning the three-phase contact line of the air–liquid interface of the trapped bubble at the tube exit and thus exposing a significant portion of oscillating interface to the outside the tube.

2. Fabrication process and experimental set-up

For the study on propulsion reversal, two types of tubes were used: commercially available capillary tubes and microfabricated tubes, as mentioned earlier.

2.1. Capillary tube swimmer

A commercially available micro glass capillary with the inner diameter of 300 μm and outer diameter of 600 μm was cut into the tubes of 1.2 mm long, and one end of the tube was sealed by thermal heating. For the stable entrapment of an air bubble inside the capillary tube, the inner and outer surface of the tube was thoroughly coated by dipping it into a Teflon solution. Once an air bubble was trapped, propulsion behaviors of this tube were examined.

2.2. Microfabricated micro swimmer

Micro swimmers embedded with micro tubes were fabricated through standard micro photolithography. The parylene C structure as a backbone of micro swimmer was deposited by the chemical vapor deposition process. The entire process is illustrated in figure 2. First, a layer of 7 μm thick parylene was deposited on a 4$''$ silicon wafer for the bottom layer of micro swimmer, followed by depositing and patterning a sacrificial layer of AZ P4620 photoresist to define the rectangular cavities of micro tubes with the dimension of 80 μm in width, 45 μm in height, and 500–2000 μm in length. Secondly, another layer of 7 μm parylene was deposited for the top and side walls of the micro tubes. Then, the reactive ion etching (RIE) process opened one end of the micro tubes and cut the outer edges of micro swimmers. The RIE process was conducted with O_2 flow rate of 50 sccm, pressure at 200 mTorr, and power at 100 W for 8 min. In this process, a sputter-coated gold layer was used as a masking layer. Afterward, the sacrificial photoresist layer was removed by acetone, and the entire body of micro swimmers was detached from the substrate at the same time, followed by rinsing with DI water.

2.3. Controlling of bubble position and length

Pinning the location of bubble interface at a desired location was done by two methods. The first method is to introduce a geometrical structure (bottle neck). The neck acts as an energy barrier (stopper) stopping the water wetting right at the neck by re-directing the dominant interfacial tension [36]. Various designs of the neck were incorporated to the micro tube opening, as shown in figure 3, by introducing a rounded neck

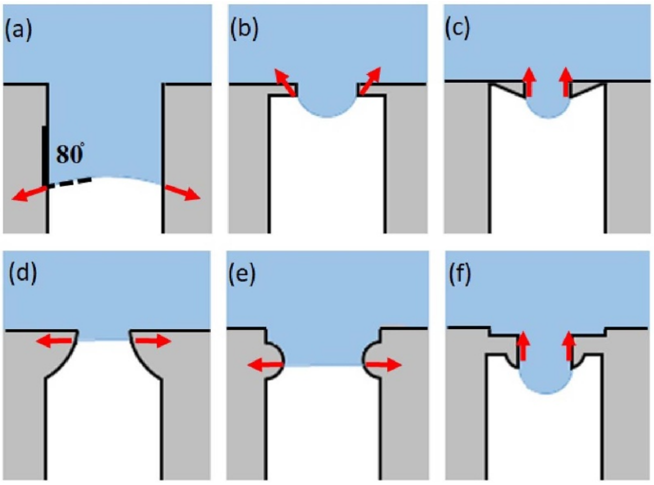

Figure 3. The entrance structures of the micro tube for micro swimmer. The white region denotes the air bubble trapped inside the tube, and the blue part denotes water. Red arrows indicate the direction of interfacial tension: (a) no neck; (b)–(f) various designs of neck.

(figure 3(e)) or sharp corners (figures 3(c), (d) and (f)) with different corner angles and directions. For all the designs, the necks are 40 μm wide located at 50 μm inside from the tube exit. As a result, the positions of three-phase contact line of the interface were well pinned at a desired location inside the tube, and the overall bubble lengths were consistently determined. The second method is to enhance hydrophobicity by treating and modifying the tube surface with SF_6 plasma two times: after the deposition of the first parylene layer and removal of the gold masking layer (figure 2). Each SF_6 plasma treatment was made for 3 min using the RIE process set at 200 mTorr in pressure, 100 W in power and 50 sccm in flow rate [37].

2.4. Swimmer testing and flow visualization

The testing of propulsion for the capillary tube swimmers and micro swimmers was done in water tanks. The capillary swimmers were tested in a water tank built up by acrylic plates (5×10 cm^2) filled with water (viscosity: 1.0×10^{-3} Pa s) or water/glycerine mixture (viscosity: 3.5×10^{-3} Pa s) to simulate the fluid dynamics in blood. The acrylic tank for the micro swimmer testing had a base area of 10×10 cm^2 and was filled with DI water (depth = 3 cm). A piezoelectric disk (AB3526B-LW100-R, PUI Audio, Inc., USA) with the diameter of 35 mm was glued onto the side wall of each water tank and connected to an amplifier and a function generator to produce acoustic waves. The amplitudes of bubble oscillation were measured using a high-speed camera (Phantom v7.3, Vision Research, Inc., USA). The flow field near the entrances of micro tubes were visualized by 8 μm glass beads. The motion of beads was tracked by the commercial visual analysis software Fiji and its plugin TrackMate. In a series of the experiments on microstreaming flows, the significance of the acoustic radiation force was checked, as follows. Under the same acoustic excitation condition, two identical tubes with and without a bubble trapped were tested. We could not observe any motion in the tube without a bubble, which indicates that the acoustic radiation force from the environment is negligible. In addition, the propulsion force by microstreaming was estimated to be $\sim\mu$N per tube (bubble) in the previous studies [25, 30]. In comparison, the acoustic radiation force from oscillation bubble exerted on cross-sectional area in the axial direction is roughly estimated to be $\sim$nN according to the analysis of Nyborg's [38] and Eller's [39] studies, which is much lower than the propulsion by microstreaming.

3. Results and discussions

3.1. Capillary tube swimmer

It has been known that when the oscillating Reynolds number Re_{osc} is high ($>\sim 100$), an oscillating gaseous bubble trapped in a one-end-open tube omnidirectionally draws the surrounding liquid into the tube during the intake period and expels it along the axial direction during the exhaust period [25]. It results in a net liquid jet flow in the outward direction from the tube when averaged over oscillation cycles, leading to propelling the tube in the opposite direction. While testing the capillary tube swimmers, a flow reversal in microstreaming and thus a backward propulsion occur most frequently when the bubble interface is completely exposed to the outside of the tube. The effect of the interface position relative to the opening of tubes on the propulsion direction is presented by sequential snapshots during the capillary swimmer propelled under the same acoustic field in figure 4. In figure 4(a), the bubble interface is located inside the tube over the whole actuation period (supplement 1 (available online at stacks.iop.org/JMM/31/084001/mmedia)); while in figure 4(b) the interface is located outside of the tube with the three-phase contact line pinned at the edge of the tube exit (supplement 2). The former (figure 4(a)) shows that the microstreaming flow is in the outgoing direction from the opening of the tube, thus generating a forward propulsion to the swimmer. In contrast, the latter (figure 4(b)) shows a propulsion reversal.

For a wide range of the actuation voltage to the piezo-actuator, the propulsion speed and direction were measured in DI water for two configurations of bubble interface (figure 5(a)). To simulate the performance of the present swimmer in blood, the swimmer was examined in a mixture of water and glycerine that has a similar viscosity of blood (3.5×10^{-3} Pa s, figure 5(b)). In both fluids, the propulsion speed generally increases as the voltage is increased. This is consistent with the previous study [25]. In addition, in the high viscosity solution (water/glycerine mixture), the propulsion speed (figure 5(b)) is overall slower than that in figure 5(a) under the same actuation voltage. This is mainly because of the increase in the drag force induced when the swimmer moves through the surrounding mixture fluid that has over three times higher viscosity than that of water. Interestingly, a reversal in the propulsion direction occurs in a quite wide window of the applied voltage between 10 and 30 V in both liquids when the interfaces are situated outside of the tube. The previous studies with oscillating sessile bubbles on the flat solid surface reported a variety of the microstreaming flow modes [8, 17, 40–42],

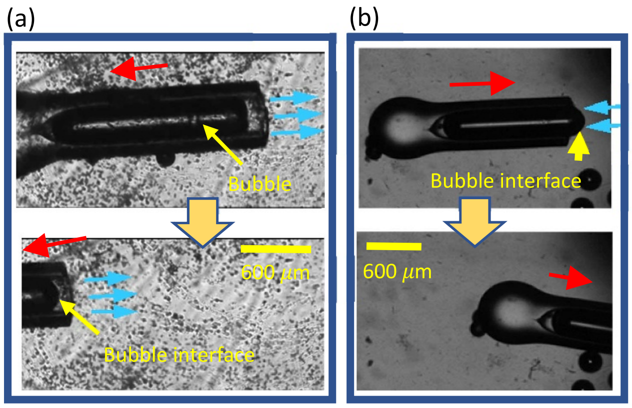

Figure 4. (a) Forward propulsion (supplement 1) and (b) backward (supplement 2) propulsion in the water-glycerine mixture (3.3 kHz, 25 V to the piezo-disk). The position of gas–liquid interface relative to the tube exit affects the propulsion direction. The blue and red arrows denote the directions of microstreaming flows and thrusts, respectively.

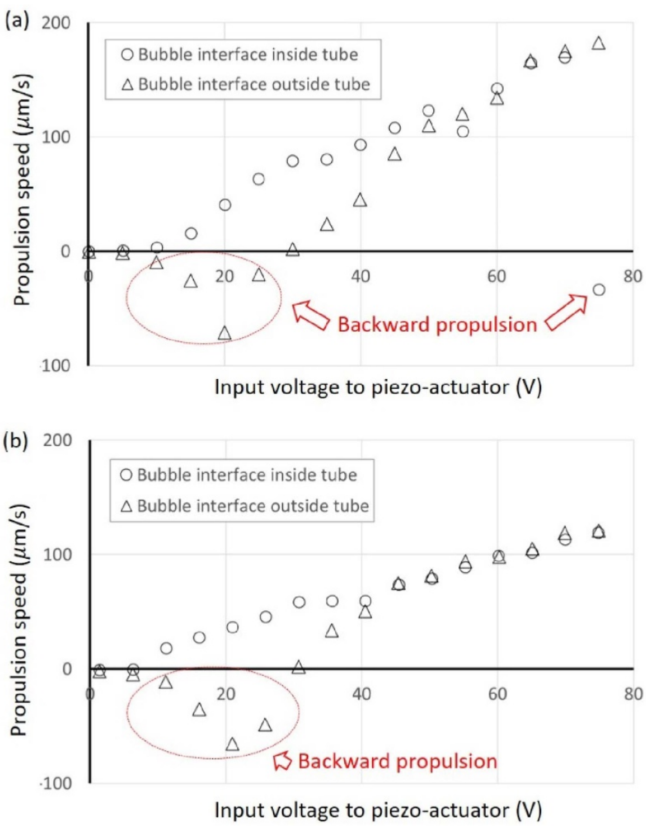

Figure 5. Propulsion speed vs input voltage to the piezo-disk; (a) propulsion in water (viscosity 1.0×10^{-3} Pa s, actuation frequency: 2.9 kHz), and (b) propulsion in a mixture of water and glycerine (viscosity 3.5×10^{-3} Pa s, similar level to blood viscosity, actuation frequency: 3.3 kHz).

which highly depend on the multiple parameters including the amplitude, frequency, etc. At this point, neither the detailed mechanism is clearly understood nor a universal law or model to predict them is established, to the authors' best knowledge. In particular, some of the patterns show reversed flow patterns,

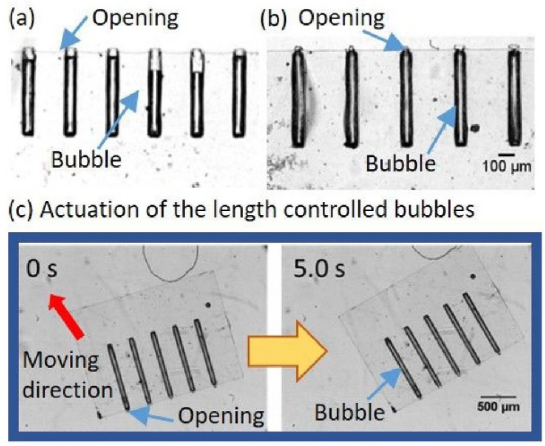

Figure 6. The micro swimmer under water (a) without and (b) with neck structures. (c) The movement of micro swimmer for 5 s under the actuation of 6.3 kHz and 150 V (supplement 3).

which may be connected to the present propulsion reversal. In the present experiment, the testing results show that the flow reversal and thus prolusion reversal likely occur when the bubble is pinned at the edge of the tube exit such that the entire part of the bubble is outside of the tube. Meanwhile, a reversal flow, although weak, appears around 75 V even with the interface initially sitting inside the tube (figure 5(a)). This may be caused by the extension of the bubble interface to the outside of the tube opening due to the large oscillation amplitude.

3.2. Micro swimmer with necking tubes

The above results imply that the position of the bubble interface relative to the tube exit is very important. However, the position is determined randomly by the surface properties (hydrophobicity, roughness, etc) and tube geometry when the dried tube is submerged into water [25, 30, 43]. Controlling the interface position with the commercial capillary tubes is very difficult. Hence, we utilized the microfabrication method with parylene for the tube body in order to have finer control over the interface position. When a bubble is trapped inside the micromachined parylene micro tube, the air–water interface is concave viewing from the water side because the intrinsic contact angle of parylene is about 80° which is less than 90°, as illustrated in figure 3(a). As a consequence, the interfacial tension points inward and draws water into the micro tube when the tube wall is straight, as shown in figure 6(a). However, owing to the variation mainly in the surface roughness of the inner wall of micro tubes, the positions of interface are randomly positioned and different among all six micro tubes, although they are fabricated under the same fabrication batch. Thus, the lengths of trapped bubbles are not uniform. This nonuniformity in the bubble length makes it difficult to predict the resonance frequency of each bubble.

On the contrary, figure 6(b) shows that the interface positions and bubble lengths are uniform when five different neck structures are incorporated into the micro tubes. Note that the five different neck designs in figures 3(b)–(f) are applied to

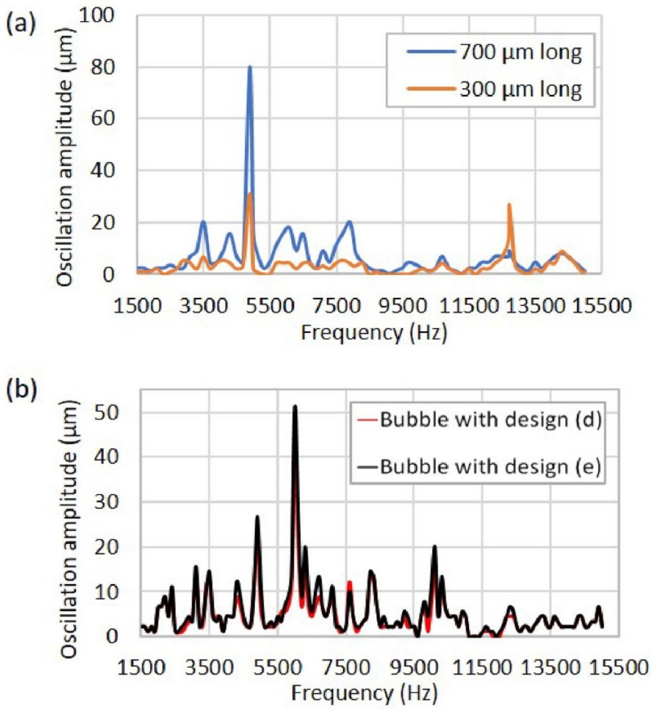

Figure 7. Spectra of oscillation amplitudes: (a) without neck designs (bubbles 700 long and 300 μm long); (b) with neck designs shown in figures 3(d) and (e) (two bubble lengths identical to 1200 μm).

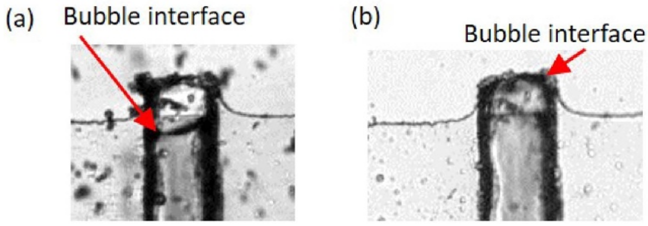

Figure 8. The opening of microtubes on micro swimmer (a) without and (b) with the surface treatment by SF_6 plasma.

the five micro tubes in the micro swimmer from left to right in the same order. All the five neck designs successfully pin the air–water interfaces on the necks, which are very close to the tube exit but still inside the tube (bubble lengths ~930 μm). It does not seem that there is any distint difference in pinning behavior among the designs. The trapped bubbles are oscillated by applying an acoustic wave at 6.3 kHz and 150 V. Sequential images of its motion are taken over a period of 5 s, and the comparison between the initial and final positions is shown in figure 6(c) (supplement 3). The micro swimmer with the five tubes is propelled over the distance of a few hundred micrometers while all the interfaces remain pinned at the necks, although the swimming route is not completely straight due to the non-uniform friction from the bottom of the tank. In addition, it seems that the most left tube in figure 6(c) (the design in figure 3(f)) is not completely open due to the complex geometry (maybe beyond the current photolithography resolution). This might be another reason why the micro swimmer is rotated while moving.

To demonstrate the impact of the bubble length on its oscillating behavior, the oscillation amplitudes of bubble interface are measured at the fixed voltage but with varying the frequency from 1.5 to 15 kHz by an equal increment of 0.1 kHz, as shown in figure 7. Regardless of the length, every bubble has a distinct peak at 4.9 kHz, which corresponds to the natural frequency of the entire system including the tank with the water and actuator. Therefore, this peak frequency will be excluded from the discussion on the bubble behavior responding to the external acoustic field. Figure 7(a) shows the spectra for two bubbles trapped in the two tubes without the neck structure, respectively. Note that even though the dimensions of the two tubes are identically designed and embedded in the same swimmer body, the final bubble lengths are significantly different: one is 300 μm long and the other is 700 μm long. This is another example of random bubble length in the bubble trapping without any control method implemented. Since the two bubbles are in the same micro swimmer, it is assumed that they are actuated under the same acoustic input. The spectra in figure 7(a) show that the 700 μm bubble is more active in the low frequency region and has the natural frequency at 8 kHz; on the other hand, the 300 μm bubble resonates at 12.7 kHz and does not noticeably respond in the low frequency range. In figure 7(b), on the other hand, two bubbles with the neck structures (designs (d) and (e) in figure 3) embedded in the same micro swimmer have the same length as 1200 μm, thus showing almost identical responses to the frequency over the entire range tested. The natural frequencies of the two bubble are identical to be 6.3 kHz.

3.3. Micro swimmer with plasma treatment

The above neck designs in the micro tube are very efficient to make the bubble length uniform and thus generate consistent spectra in the oscillation amplitude. However, since the interfaces of bubble are still located inside the tubes, any reversal in microstreaming or propulsion force is not observed. To see if there exists any flow reversal with the micro tubes, similar to the capillary tube case, the surface of the micro tube is treated by SF_6 plasma. Figure 8 shows two openings of micro tubes: without (figure 8(a)) and with (figure 8(b)) the surface treatment by SF_6 plasma. Figure 8(a) shows a clear boundary between the gas and liquid phase is located inside the microtube. In contrast, the micro tube in figure 8(b), treated by SF_6 plasma, is completely filled with the bubble, and thus the interface of the bubble is outside of the tube, due to the enhanced hydrophobicity. The swimming motion in figure 9 shows that the micro swimmer with the plasma treated tubes (750 μm long) exhibits a reverse propulsion at the speed of 2.1 mm s^{-1} (supplement 4, input signal to the piezo-disk: 6.9 kHz and 59.4 V). That is, a pulling force is generated. Recall from figure 6(c) that the micro swimmer propels forward when the bubble interface is pinned at the neck inside the micro tube.

The flow fields for over a 10 s period near these two types of tubes were visualized by tracking seeded particles (8 μm glass beads) and presented in figure 10. Both mico tubes in

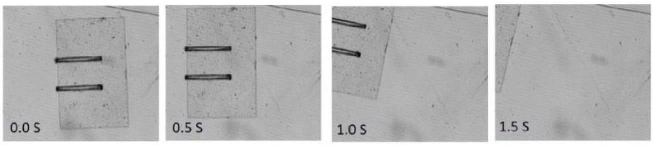

Figure 9. A sequential image series of the movement of micro swimmer with the bubble interface staying outside of the micro tubes (supplement 4).

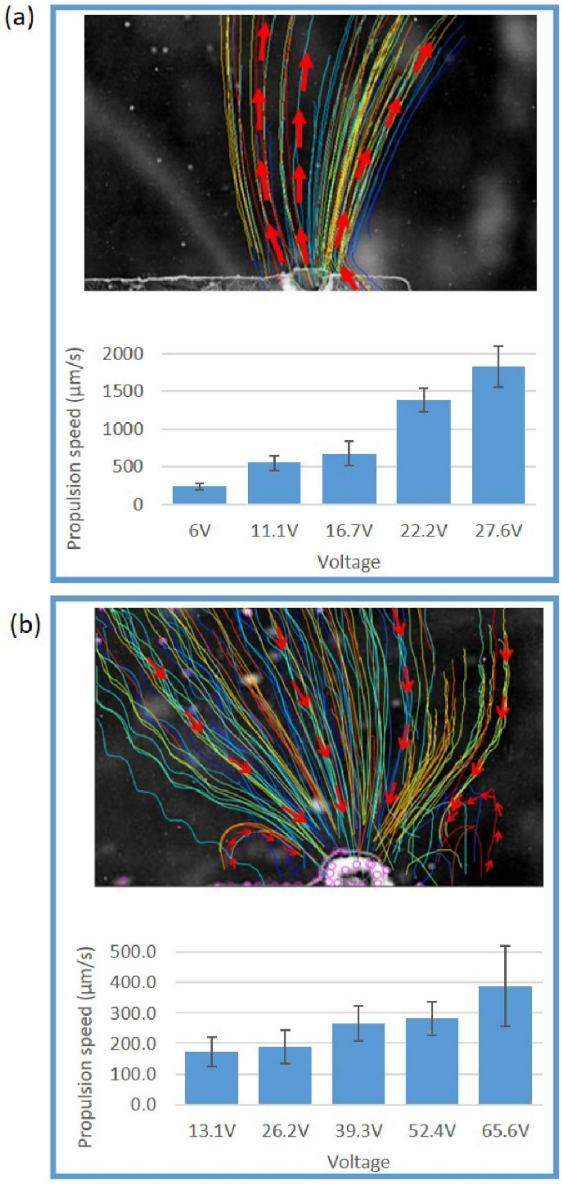

Figure 10. The visualization of the microstreaming flow by particle tracking and the propulsion speed under different actuation voltages of micro swimmer: (a) the bubble interface is inside the tube. The microstreaming flow is outgoing from the tube exit, generating a pushing force; (b) the bubble interface is outside of the tube. The microstreaming flow is towards the tube exit and generates a pulling force.

figures 10(a) and (b) are 480 μm long and 80 μm wide without any neck structure. The micro tube in figure 10(a) has no SF_6 plasma treatment during the fabrication and thus trapped the air bubble at the length of 320 μm which has its interface located inside the microtube. On the otherhand, the micro tube in figure 10(b) has two SF_6 treatments during the fabrication, as shown in figure 2, and traps an air bubble completely filling the microtube (the bubble length identical to the tube length). The microstreaming flow goes outward along the axial direction of the tube (figure 10(a), top) when the bubble interface stays inside the micro tube during the whole period of oscillation (signal to the piezo-disk: 10.3 kHz, 22 V), thus propelling the micro swimmer in the opposite direction to the flow (forward). By contrary, the microstreaming flow direction is towards the tube exit when the bubble interface is completely outside of the micro tube (figure 10(b), top). The micro swimmer is drawn backward (signal to the piezo-disk: 7.6 kHz, 55 V). More quantitative measurements are made to find the relation of the propulsion speed to the applied voltage, as shown in figures 10(a) and (b) bottom. Both forward and backward propulsion speeds are proportional to the applied voltage. Unlike the capillary tube case, the reversal propulsion persists even in the high voltage range when the interface is situated out of the tube. However, the forward propulsion speed reaches higher and requires lower voltages than the backward propulsion case. This may be due to the fact that the oscillating interface is more stable when it is inside the tube since the interface is confined and surrounded by the tube wall. The generated microstreaming flow is more focused axially. When the bubble interface is outside of the tube, it is observed that the oscillating bubble is likely to separate and escape from the micro tube as the applied voltage increases.

4. Conclusion

A gaseous bubble in liquid oscillates under the presence of acoustic waves because it is compressible. In particular, an acoustically oscillating bubble which is trapped in a one-end-open tube is capable of producing significant microstreaming axial flows along the tube and thus generating a propulsion force to the tube by reaction when the oscillating frequency is high enough for inertia effects to come into play. This article reports that the microstreaming flow and propulsion can be reversed in the condition where the position of air–bubble interface is pinned at the tube exit. Such propulsion reversal with the tube-trapped bubble has not or rarely been reported previously, to the authors' best knowledge. This phenomenon is confirmed occurring with both commercially available capillary glass tubes (a certain range of applied voltage) and microfabricated parylene tubes (the entire testing range of applied voltage) when the trapped bubbles oscillate resonantly.

This finding implies that controlling the interface position and bubble length is critically important to generate consistent propulsion in a predictable manner. As such, two methods are incorporated to pin the interface at a desired location in a controlled manner. The first method is to introduce neck structures at the tube exit such that the bubble interface is always pinned at the neck structure near the tube exit and the bubble length becomes uniform. This uniform length of bubbles generates a consistent oscillating spectrum under acoustic excitation. This outcome provides advantages of more precise and repeatable propulsion performance of the micro swimmer. However, the reversal in microstreaming flow and propulsion is not observed with these neck-implemented tubes since the bubble interface still stays inside the tube. The second method is to treat the microfabricated tube with SF_6 plasma such that the surface of the tube becomes more hydrophobic. This enables that the trapped bubble is not only pinned right at the edge of the tube exit but the entire gas–liquid interface is also exposed to the outside of tube. In this condition, the reversal in the microstreaming flow as well as propulsion can be generated. The present results of propulsion reversal can not only spark more follow-up research activities in theoretical, numerical, and experimental aspects to understand the phenomena better but also provide more options in controlling and maneuvering the bubble-powered micro swimmer when applied.

Data availability statement

The data that support the findings of this study are available upon reasonable request from the authors.

Acknowledgment

This work was supported by the National Science Foundation projects (NSF ECCS-1637815 and 1951051)

ORCID iD

Sung Kwon Cho https://orcid.org/0000-0001-7283-8839

References

[1] Rayleigh L 1917 On the pressure developed in a liquid during the collapse of a spherical cavity *Phil. Mag.* **34** 94–8
[2] Neppiras E A 1980 Acoustic cavitation *Phys. Rep.* **61** 159–251
[3] Lighthill S J 1978 Acoustic streaming *J. Sound Vib.* **61** 391–418
[4] Nyborg W L 1958 Acoustic streaming near a boundary *J. Acoust. Soc. Am.* **30** 329–39
[5] Nyborg W L, Gould R K and Jackson F J 1959 Sonically induced microstreaming applied to a surface reaction *J. Acoust. Soc. Am.* **31** 706–11
[6] Brennen C E 1995 *Cavitation and Bubble Dynamics* (Oxford: Oxford University Press)
[7] Oğuz H and Prosperetti A 1998 The natural frequency of oscillation of gas bubbles in tubes *J. Acoust. Soc. Am.* **103** 3301–8
[8] Ryu K, Chung S K and Cho S K 2010 Micropumping by an acoustically excited oscillating bubble for automated implantable microfluidic devices *J. Lab. Autom.* **15** 163–71
[9] Tovar A R, Patel M V and Lee A P 2011 Lateral air cavities for microfluidic pumping with the use of acoustic energy *Microfluid. Nanofluid.* **10** 1269–78
[10] Gao Y, Wu M, Lin Y, Zhao W and Xu J 2020 Acoustic bubble-based bidirectional micropump *Microfluid. Nanofluid.* **24** 1–10
[11] Liu R, Lenigk R, Druyor-Sanchez R, Yang J and Grodzinski P 2003 Hybridization enhancement using cavitation microstreaming *Anal. Chem.* **75** 1911–7
[12] Mao X, Juluri B K, Lapsley M I and Huang T J 2008 Milliseconds microfluidic bubble mixer using chaotic advection *Proc. ASME Int. Mechanical Engineering Congress and Exposition* (Boston, MA: Nano-Manufacturing Technology) pp 927–30
[13] Ahmed D, Mao X, Juluri B K and Huang T J 2009 A fast microfluidic mixer based on acoustically driven sidewall-trapped microbubbles *Microfluid. Nanofluid.* **7** 727–31
[14] Okabe Y, Chen Y, Purohit R, Corn R M and Lee A P 2012 Piezoelectrically driven vertical cavity acoustic transducers for the convective transport and rapid detection of DNA and protein binding to DNA microarrays with SPR imaging—a parametric study *Biosens. Bioelectron.* **35** 37–43
[15] Ozcelik A, Ahmed D, Xie Y, Nama N, Qu Z, Nawaz A A and Huang T J 2014 An acoustofluidic micromixer via bubble inception and cavitation from microchannel sidewalls *Anal. Chem.* **86** 5083–8
[16] Orbay S, Ozcelik A, Lata J, Kaynak M, Wu M and Huang T J 2016 Mixing high-viscosity fluids via acoustically driven bubbles *J. Micromech. Microeng.* **27** 015008
[17] Marmottant P and Hilgenfeldt S 2003 Controlled vesicle deformation and lysis by single oscillating bubbles *Nature* **423** 153–6
[18] Chung S K and Cho S K 2008 On-chip manipulation of objects using mobile oscillating bubbles *J. Micromech. Microeng.* **18** 125024
[19] Chung S K and Cho S K 2009 3D manipulation of millimeter- and micro-sized objects using an acoustically excited oscillating bubble *Microfluid. Nanofluid.* **6** 261–5
[20] Rogers P and Neild A 2011 Selective particle trapping using an oscillating microbubble *Lab Chip* **11** 3710–5
[21] Patel M V, Tovara A R and Lee A P 2012 Lateral cavity acoustic transducer as an on-chip cell/particle microfluidic switch *Lab Chip* **12** 139–45
[22] Tandiono T, Ow D S W, Driessen L, Chin C S H, Klaseboer E, Choo A B H, Ohla S W and Ohl C D 2012 Sonolysis of Escherichia coli and Pichia pastoris in microfluidics *Lab Chip* **12** 780–6
[23] Phan H V, Sesen M, Alan T and Neild A 2014 Single line particle focusing using a vibrating bubble *Appl. Phys. Lett.* **105** 193507
[24] Purcell E M 1977 Life at low Reynolds number *Am. J. Phys.* **45** 3–11
[25] Feng J, Yuan J and Cho S K 2015 Micropropulsion by an acoustic bubble for navigating microfluidic spaces *Lab Chip* **15** 1554–62
[26] Ceylan H, Giltinan J, Kozielskia K and Sitti M 2017 Mobile microrobots for bioengineering applications *Lab Chip* **17** 1705–24
[27] Dijkink R, Van Der Dennen J, Ohl C and Prosperetti A 2006 The 'acoustic scallop': a bubble-powered actuator *J. Micromech. Microeng.* **16** 1653–9
[28] Feng J and Cho S K 2013 Micro propulsion in liquid by oscillating bubbles *26th Int. Conf. Micro Electro Mech. Syst. (MEMS)* (*Taipei, Taiwan*, *20–24 January*) pp 63–6
[29] Feng J and Cho S K 2014 Two-dimensionally steering microswimmer propelled by oscillating bubbles *27th Int. Conf. Micro Electro Mech. Syst. (MEMS)* (*San Francisco, CA, USA*, *26–28 January*) pp 188–91
[30] Feng J, Yuan J and Cho S K 2016 2D steering and propelling of acoustic bubblepowered microswimmers *Lab Chip* **16** 2317–25
[31] Liu F W and Cho S K 2019 3D micro swimming drone with maneuverability *32nd Int. Conf. Micro Electro Mech. Syst. (MEMS)* (*Seoul, South Korea*, *27–31 January*) pp 10–3

[32] Liu F W and Cho S K 2021 3D swimming microdrone powered by acoustic bubbles *Lab Chip* **21** 355–64
[33] Ahmed D, Lu M, Nourhani A, Lammert P E, Stratton Z, Muddana H S, Crespi V H and Huang T J 2015 Selectively manipulable acoustic-powered microswimmers *Sci. Rep.* **5** 9744–51
[34] Louf J F, Bertin N, Dollet B, Stephan O and Marmottant P 2018 Hovering microswimmers exhibit ultrafast motion to navigate under acoustic forces *Adv. Mater. Interfaces* **5** 1800425
[35] Ren L, Nama N, McNeill J M, Soto F, Yan Z, Liu W, Wang W, Wang J and Mallouk T E 2019 3D steerable, acoustically powered microswimmers for single-particle manipulation *Sci. Adv.* **5** eaax3084
[36] Liu T and Kim C J 2014 Turning a surface superrepellent even to completely wetting liquids *Science* **346** 1096–110
[37] Bi X, Crum B P and Li W 2014 Super hydrophobic parylene-C produced by consecutive O_2 and SF_6 plasma treatment *J. Microelectromech. Syst.* **23** 628–35
[38] Nyborg W L 1982 Ultrasonic microstreaming and related phenomena *Br. J. Cancer* **45** 156–60
[39] Eller A 1968 Force on a bubble in a standing acoustic wave *J. Acoust. Soc. Am.* **43** 170–2
[40] Marmottant P, Raven J, Gardeniers H, Bomber J and Hilgenfeldt S 2006 Microfluidics with ultrasound-driven bubbles *J. Fluid Mech.* **568** 109–18
[41] Tho P, Manasseh R and Ooi A 2007 Cavitation microstreaming patterns in single and multiple bubble systems *J. Fluid Mech.* **576** 191–233
[42] Jalal J and Leong T S H 2018 Microstreaming and its role in applications: a mini-review *Fluids* **3** 93
[43] Bertin N, Spelman T A, Stephan O, Gredy L, Bouriau M, Lauga E and Marmottant P 2015 Propulsion of bubble-based acoustic microswimmers *Phys. Rev. Appl.* **4** 064012